

Washington University in St. Louis

## Washington University Open Scholarship

---

Senior Honors Papers / Undergraduate Theses

Undergraduate Research

---

Spring 5-8-2024

### Role of Integrase-PP2A Interaction in Human T-Cell Leukemia Virus Type-1 Replication and Pathogenesis

Shayna Turbin

Follow this and additional works at: [https://openscholarship.wustl.edu/undergrad\\_etd](https://openscholarship.wustl.edu/undergrad_etd)



Part of the [Biology Commons](#), [Oncology Commons](#), and the [Virology Commons](#)

---

#### Recommended Citation

Turbin, Shayna, "Role of Integrase-PP2A Interaction in Human T-Cell Leukemia Virus Type-1 Replication and Pathogenesis" (2024). *Senior Honors Papers / Undergraduate Theses*. 63.  
[https://openscholarship.wustl.edu/undergrad\\_etd/63](https://openscholarship.wustl.edu/undergrad_etd/63)

This Unrestricted is brought to you for free and open access by the Undergraduate Research at Washington University Open Scholarship. It has been accepted for inclusion in Senior Honors Papers / Undergraduate Theses by an authorized administrator of Washington University Open Scholarship. For more information, please contact [digital@wumail.wustl.edu](mailto:digital@wumail.wustl.edu).

Role of Integrase-PP2A Interaction in Human T-Cell Leukemia Virus Type-1  
Replication and Pathogenesis

by  
Shayna Ellie Turbin

Mentor Names:  
Xiaogang Cheng, PhD  
Nehla Banu, PhD  
Lee Ratner, MD, PhD

John T. Milliken Department of Medicine  
Division of Oncology

Spring 2024

## **Table of Contents**

Abstract.....	4
Acknowledgements.....	5
1. INTRODUCTION .....	6
1.1 HTLV Overview.....	6
1.2 HTLV-Associated Diseases.....	7
1.3 Transmission of HTLV-1.....	7
1.4 HTLV Genome and Structure .....	9
1.5 Cell Infection .....	10
1.6 Retroviral Integrase.....	11
1.7 Protein Phosphatase 2A (PP2A).....	13
1.8 Integrase and PP2A B'56 $\gamma$ Subunit.....	15
1.9 Hypothesis.....	16
2. MATERIALS AND METHODS .....	17
2.1 Mutant Virus and Cell Lines .....	17
2.2 Transforming <i>E. coli</i> with plasmid DNA.....	17
2.3 Isolating plasmid DNA .....	18
2.4 Plasmid Linearization .....	20
2.5 Transfecting 729B Cells.....	21
2.6 p19 HTLV-1 ELISA assay .....	22
2.7 Single Cell Cloning.....	23
2.8 Quantifying p19 Positive Single Clone Viral Particle Production.....	23
2.9 Infection assays.....	23
2.10 Confirming Integrase Mutation and Full-Length Viral Genome .....	24
2.11 Western Blot.....	26
3. RESULTS.....	28
3.1 Establishing stable 729B-ACH cell lines that produce infectious HTLV-1 virus .....	28
3.2 The 729B-ACH cell clones carry the full length proviral genome and correct integrase gene sequence. ....	30
3.3 The mutations in the integrase LxxIx $\epsilon$ motif inhibit HTLV-1 infection. ....	32

3.4 The integrase mutations of the provirus did not change the viral protein synthesis and packaging in 729B-ACH cell clones.....	34
4. DISCUSSION.....	37
References.....	40

## **Abstract**

Human T-cell leukemia virus type-1 (HTLV-1) is an oncogenic retrovirus that causes multiple disorders, including adult T-cell leukemia and HTLV-1-associated myelopathy/tropical spastic paraparesis. HTLV-1 retroviral integrase binds to the regulatory B'56 $\gamma$  subunit of the host cell Protein Phosphatase 2A (PP2A). Integrase contains a highly conserved LxxIxE motif that is essential for binding, which increases integration efficiency and facilitates HTLV-1 hijack of host cell machinery. We aim to understand how mutations introduced in the highly conserved binding site can affect viral particle production and infectivity. We transfected 729B human lymphoblastoid cells and 293T cells with mutant and wildtype virus. Mutations L213A, I216A, and E218A within the LxxIxE motif interfered with integrase-PP2A binding and the D122N mutation eliminated integrase catalytic activity, serving as a negative control. Single cell clones were obtained from mutant and wildtype virus transfected cells. Virus production for each clone was determined using a p19 ELISA assay. The clones with higher and similar p19 production were selected for infectivity assays and will be used to infect humanized mice for our *in vivo* study. The binding site mutation decreased viral replication in 729B-ACH cell clones and decreased infectivity in both cell lines. We anticipate that humanized mice will exhibit slower disease progression or even no HTLV-1 infection and disease when infected with the mutant viruses. This study provides preliminary evidence for treatments that target integrase-PP2A binding since binding site mutations decreased HTLV-1 viral replication and infectivity.

## **Acknowledgements**

First and foremost, I would like to thank Dr. Xiaogang Cheng, Dr. Nehla Banu, and Dr. Lee Ratner for their unwavering support and guidance. My thesis would not have been possible without their expertise, contributions, and dedication. Over the past two and a half years, their mentorship has ignited my passion for research and has empowered me to grow as a scientist. I would like to express my deepest gratitude to Dr. Ratner for trusting me with his ideas; the opportunity to work in the Ratner Lab has been a formative experience in my undergraduate education. I am extremely thankful for the countless hours Nehla and Xiaogang have spent teaching me new skills and techniques, which I will carry with me throughout my career. I also want to credit Xiaogang and Nehla for their work to produce Figures 9, 12, 13, 14, and 15.

I am also grateful to the entirety of the Ratner Lab for feedback and support. Their encouragement, advice, and assistance were integral to the completion of this thesis and my development as a researcher. I am appreciative of the time and resources the Ratner Lab has invested in my growth.

Funding for this project was supported by Ratner Lab funding from the National Institutes of Health grants.

## 1. INTRODUCTION

### 1.1 HTLV Overview

Human T-cell leukemia virus type-1 (HTLV-1) is an oncogenic retrovirus estimated to have infected 5-10 million individuals across the globe (1). HTLV-1 belongs to the *Deltaretrovirus* genus of the *Retroviridae* family, which consists of primate T-lymphotropic viruses (PTLVs) and bovine leukemia virus (BLV) (2). BLV is a retrovirus that causes B-cell leukemia in 5% of infected cattle (3). PTLVs are retroviruses that specifically infect primates (4). PTLVs that infect human hosts are characterized as human T-cell leukemia viruses (HTLVs); PTLVs that infect nonhuman primates are classified as simian T-cell leukemia viruses (STLVs) (4).

Currently, there are four known HTLVs that infect human hosts (5). HTLV-1 is the first oncogenic human retrovirus that was identified and isolated. The Gallo laboratory discovered retrovirus particles in a patient's T-cell lymphoblastoid cell lines (6). Although HTLV was originally detected in the 1980s, researchers estimate HTLVs have infected human hosts for thousands of years, dating back to the Paleolithic Period (7). HTLV-1 has become endemic across the world, including regions of Japan, Africa, the Caribbean, South America, Northeast Iran, Australia, and Melanesia. HTLV-1 is pathogenic and causes adult T-cell leukemia (ATL) and HTLV-1-associated myelopathy/tropical spastic paraparesis (HAM/TSP). HTLV-2 is most prevalent in injection drug users and indigenous communities in the Americas, particularly in the Brazilian Amazon. Although HTLV-2 is not highly pathogenic, several cases of TSP, pneumonia, and arthritis have been reported (8). HTLV-3 and HTLV-4 were more recently discovered in Cameroon; further research is required to determine transmission patterns and the potential for viral pathogenicity (9).

## 1.2 HTLV-Associated Diseases

Since HTLV-1 has various clinical manifestations, it is the most clinically significant virus in the HTLV family and is the focus of this study (5). HTLV-1 infected individuals risk developing malignant, inflammatory, and opportunistic diseases. Approximately 5% of HTLV-1 infections cause ATL, a highly aggressive T-cell malignancy (10). ATL may present as the acute, lymphomatous, chronic, or smoldering form (5). The acute subtype is most common and has a median survival time of 6 months post diagnosis (11). Another 4% of HTLV-1 positive patients develop a chronic, progressive inflammatory disorder known as HAM/TSP that causes weakness and partial paralysis in the lower limbs (12). Individuals with high proviral loads are more likely to develop ATL and HAM/TSP (13, 14). HTLV-1 infected individuals have a higher incidence of opportunistic infections, including pneumocystis pneumonia, gastroenterocolitis, and cryptococcal meningitis as HTLV-1 affects the host's immune system (15). Although HTLV-1 infection is associated with significant morbidity and mortality, there are no vaccines and limited therapies are available. Therefore, it is crucial to investigate viral transmission, replication, and infectivity patterns to identify targets for future therapeutic interventions.

## 1.3 Transmission of HTLV-1

HTLV-1 is transmitted through direct contact between hosts via three major transmission routes (5). The predominant transmission mode is vertical transmission through breastfeeding. HTLV-1 positive mothers with high milk proviral loads, high HTLV-1 antibody serum titers, and those who breastfeed longer than 6 months are more likely to transmit HTLV-1 to their breast-fed children (16). Individuals who are infected while breastfeeding are more prone to develop ATL (17). HTLV-1 transmission also occurs through sexual intercourse. There is higher transmission

efficiency from men to women, and sexual transmission is associated with HAM/TSP (18). The third major transmission route is through contact with contaminated blood. Blood transfusions that contain HTLV-1 infected lymphocytes are associated with an increased risk of rapid seroconversion (5). Moreover, organ transplantation from HTLV positive donors to seronegative recipients may cause donor-derived infection (19). There are no universal donor screening requirements in countries such as the United States because of low HTLV prevalence and the potential for false positives amidst organ shortages. Transplant recipients on immunosuppressants have a higher risk for developing HAM/TSP and ATL; there are several case reports of HTLV-1 associated infections in kidney, heart, and liver transplant recipients from HTLV-1 positive donors (20).

After viral entry through sexual intercourse, contact with contaminated blood products, or from mother to child through breastfeeding, the transfer of live infected cells establishes initial infection in the new host (17). Infected cells disseminate HTLV-1 through direct contact with other immune cells (10). Transmission occurs across a virological synapse (VS), cellular conduits, or extracellular viral assemblies (17). A VS is a cell junction that forms from protein interaction between the infected and uninfected immune cell (17). The Microtubule Organizing Center and budding virus are polarized to direct viral transmission through the synaptic cleft to the target cell (21). The retrovirus HIV similarly hijacks host cell machinery to facilitate viral dissemination through cell-cell junctions (22). HTLV-1 transmission may also occur through cellular conduits. Cellular conduits are membrane extensions containing filamentous actin that connect T-cells to mediate HTLV-1 transfer (23). Higher viral p8 protein levels are associated with increased conduit length and number, which promotes rapid viral transmission and immune evasion (23). Cell-to-cell transmission can also occur using extracellular viral assemblies. After

budding, HTLV-1 virions are stored in extracellular structures that resemble bacterial biofilms (21). The viral biofilms can adhere to uninfected cells to facilitate viral transmission (21). Although viral transmission is more efficient through cell-cell contact between T-cells, HTLV-1 can be transmitted through free-virus particles (24). Through trans-infection, both HTLV-1 and HIV can be transmitted from dendritic cells to T-cells (24). Both cell-to-cell and cell-free transmission enable the HTLV-1 virion to contact the uninfected target cell to facilitate viral dissemination.

#### **1.4 HTLV Genome and Structure**

The HTLV-1 virion that infects the target cell is an enveloped virus with two covalently bound positive and negative sense genomic RNA strands (Figure 1) (17). The genome contains 5' and 3' long terminal repeat (LTR) sequences, that each consist of a unique 3' region (U3), a repeated region (R), and a unique 5' region (U5). For the positive sense genomic RNA, transcription is initiated in the 5' LTR (10). The positive strand encodes various structural genes, including the gag, pol, pro and env genes (17). The initial gag protein is cleaved to produce the p19 matrix protein, the p24 capsid protein, and the p15 nucleocapsid protein. The pol gene produces reverse transcriptase, RNaseH, and Integrase, and the pro gene encodes a protease. The env protein is cleaved to form the extracellular gp46 protein and the transmembrane gp21 protein. The plus strand also contains the pX region that encodes the tax and rex accessory genes (10). Alternative splicing of pX mRNA produces the p12, p13, and p30 accessory proteins (25). For the negative sense strand, transcription is initiated in the 3' LTR (10). This antisense strand encodes the HBZ gene.

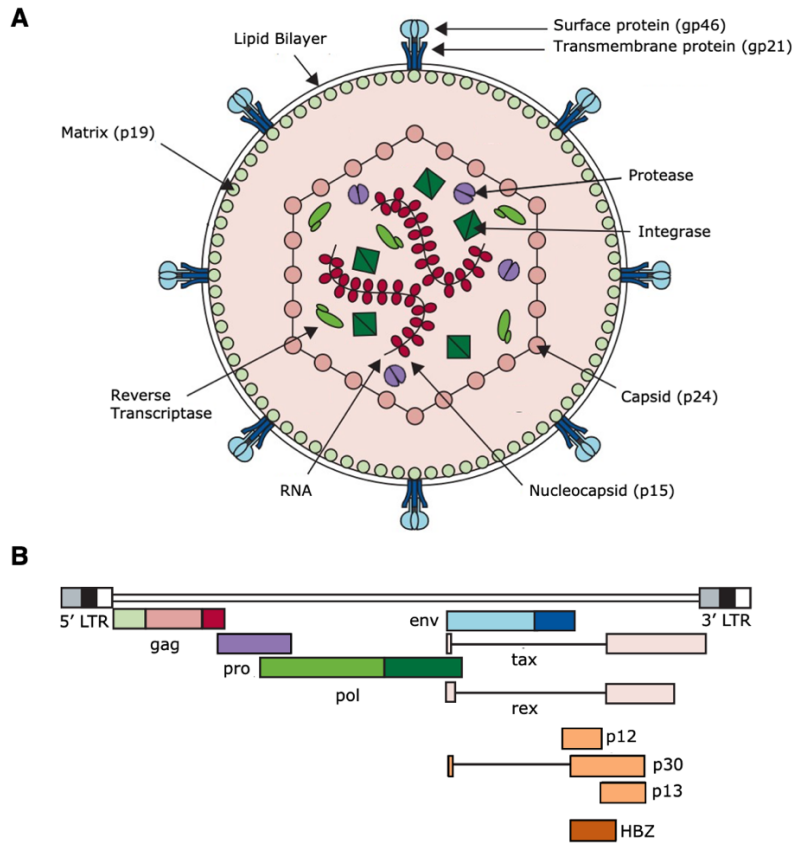


**Figure 1: HTLV-1 viral particle structure and genome architecture.**

(A) Schematic representation of HTLV-1 viral particle. The p19 matrix, p24 capsid, and p15 nucleocapsid gag protein products are labeled above. Reverse transcriptase and integrase are pol gene products located within the capsid. The pro gene encodes a protease, shown as a purple dimer. The env protein cleavage products gp46 and gp21 are shown in light and dark blue respectively. Figure is adapted from reference 26 (Verdonck *et al.*, 2007) (26). (B) Structure of HTLV-1 genome. The 5' and 3' LTR contain U3, R, and U5 regions shown in grey, black, and white respectively. The relative locations of the gag, pro, pol, env, tax, rex, p12, p30, p13, and HBZ genes are shown above. The colors of major gene products are consistent with Figure 1A. Figure is adapted from reference 26 (Verdonck *et al.*, 2007) (26).

## 1.5 Cell Infection

The virion envelope proteins bind to glucose transporter 1, neuropilin 1, and heparan sulfate proteoglycan, which are cell surface receptors that constitute the HTLV-1 receptor complex (27). This protein complex is present in various cell types, but HTLV-1 mainly targets activated CD4<sup>+</sup> T-cells (17). After the virion binds to the HTLV-1 receptor complex and fuses

with the target cell, the 9 kb viral genome enters the host cell cytoplasm. Since HTLV-1 is a retrovirus, reverse transcriptase synthesizes a complementary DNA copy of the viral RNA genome template. Integrase catalyzes the addition of the reverse transcribed DNA into the host cell's genome. HTLV-1 hijacks the host cell machinery; RNA polymerase II transcribes the integrated provirus, which is spliced, translated, and packaged to produce additional mature viral particles that can infect other immune cells. During the acute phase, HTLV-1 is mainly transmitted via cell-to-cell contact (17). The chronic stage is characterized by clonal expansion – mitotic replication from a single infected cell (17).

## **1.6 Retroviral Integrase**

Retroviral integrase has an essential role in the viral replication process and has two major catalytic functions. Integrase catalyzes the 3' end processing of viral DNA and the strand transfer reaction. During 3' processing, integrase cleaves 2-3 nucleotides from the 3' ends of the viral DNA to expose the hydroxyls bound to the invariant CA dinucleotide (28). In the strand transfer reaction, the exposed 3' hydroxyl groups break the host DNA phosphodiester bonds, and the provirus is integrated into the host cell DNA (28). HTLV-1 integration tends to occur in transcriptionally active segments of the genome, particularly sites near CpG islands (29). The retrovirus HIV-1 also has integration site specificity for transcriptionally active genes; lens epithelium-derived growth factor (LEDGF) directs the DNA copy of the HIV-1 genome to highly expressed genes for integration (30). Moreover, bromodomain proteins and the BRD2, BRD3, and BRD4 extra-terminal proteins mediate Murine Leukemia Virus integration for the gammaretrovirus in rodents (31). Further research is required to characterize the factors responsible for HTLV-1 integration at active transcription units (10).

Retroviral integrases have relatively conserved components that constitute three structural domains (32). All retroviral integrases contain a N-terminal binding domain (NTD), a catalytic core domain (CCD), and a C-terminal binding domain (CTD). The NTD contains a HHCC invariant residue sequence that coordinates zinc binding and stabilizes the structure of the amino-terminal domain. The CCD contains the longest amino acid sequence and is located between the NTD and CTD. The CCD contains the DDE invariant residue sequence and the enzyme's active site, which coordinates integrase's catalytic functions, including 3' end processing and the strand transfer reaction. The CTD has DNA-binding activity and is the least conserved domain between retroviral integrases; the most significant difference between HTLV and HIV retroviral integrases are within the CTD (Figure 2). The NTD, CCD, and CTD are connected with flexible linkers that enable integrase to maintain its three-dimensional structure (32).

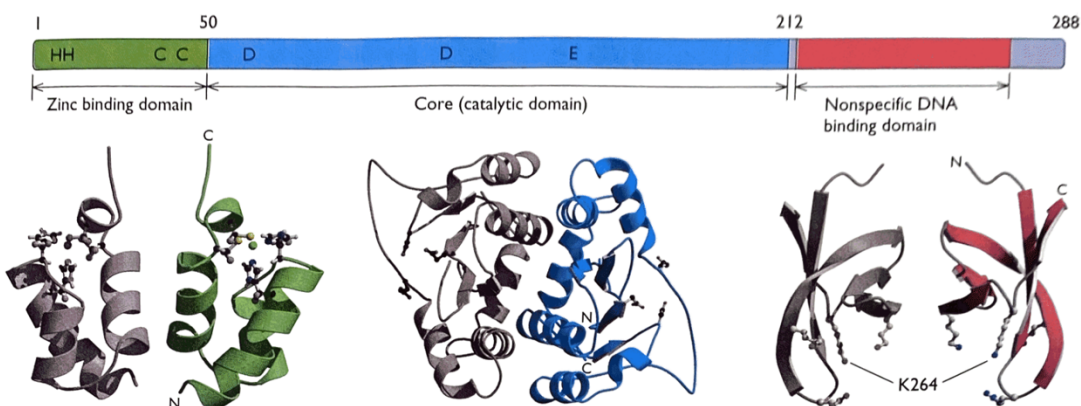


**Figure 2: HIV-1 retroviral integrase.**

HIV-1 integrase consists of a N-terminal domain (shown in green), a catalytic core domain (shown in blue), and a C-terminal DNA binding domain (shown in red). Overall, retroviral integrases have highly conserved structures. The primary differences between HTLV-1 and HIV-1 integrase are within the C-terminal DNA binding domain. Figure is from reference 33 (Flint *et al.* 1999) (33)

For integration to occur, integrase forms a stable intasome complex (34). The HTLV-1 intasome has a twofold symmetric structure and contains an integrase tetramer with two inner catalytic and two outer non-catalytic subunits. The nucleoprotein structure contains host co-factors that facilitate the integration process. HIV-1 integrase binds the host LEDGF nuclear protein, and current HIV antiviral drugs target this binding process. HTLV-1 integrase binds the host protein phosphatase 2A (PP2A); this interaction is essential for stable intasome assembly in  $\delta$ -retroviruses and increases integration efficiency (35).

### **1.7 Protein Phosphatase 2A (PP2A)**

PP2A is a ubiquitous, heterotrimeric host cell protein that is responsible for the vast majority of serine/threonine phosphatase activity (36). PP2A is a master regulator of the cell cycle and is therefore involved in essential cellular processes, including cell proliferation and death, cell mobility, and cytoskeleton dynamics. The serine/threonine protein kinase is also implicated in mitosis, DNA replication, signal transduction, translation, and heat-shock responses (36). PP2A is mostly known as a tumor suppressor and its inhibition, which is caused by mutations and deregulation, is associated with tumorigenesis (37). It is no surprise that viruses have evolved to target PP2A via several different mechanisms to modulate its phosphatase activity and downstream signaling functions to subsequently enhance viral replication. PP2A has an integral role in DNA damage repair (DDR) pathways (38). PP2A recruits DNA repair proteins and activates several primary and secondary kinases to facilitate DDR. There is recent evidence that HIV-1 hijacks traditional DDR pathways to promote viral replication, successful integration, and diminish immune responses. The HIV-1 accessory protein Vif is a PP2A antagonist; upon binding to the PP2A-B56 complex, Vif specifically inhibits the ATM DNA repair kinase and hinders single-strand and double-strand DNA break repair. Vif also interferes with host antiviral

defense mechanisms by preventing ATM activation of NF- $\kappa$ B pro-inflammatory signaling and the phosphorylation of TRIM antiviral proteins (38).

The PP2A heterotrimer contains a structural A subunit, a regulatory B subunit, and a catalytic C subunit (36). The A subunit acts as a scaffold for B subunit binding. The  $\alpha$  and  $\beta$  isoforms of the A subunit are both expressed in mammals and have similar sequence identity. The C subunits have catalytic functions and also have  $\alpha$  and  $\beta$  isoforms. The regulatory B subunits have dissimilar sequences and include four distinct subunit families. Either the B, B', B'', or B''' subunit family, which bind to the scaffold provided by the A and C subunit. The B' family interacts with HTLV-1 integrase and is the focus of this study (35). The B' family has  $\alpha$ ,  $\beta$ ,  $\gamma$ ,  $\delta$  and  $\epsilon$  variants (36). Delta-retroviral integrase specifically binds to the B'56 $\gamma$  structural subunit, which stabilizes the HTLV-1 intasome structure and promotes HTLV-1 integration efficiency (34).

The PP2A B56 subunit has substrate specificity for binding proteins with a conserved LxxIxE motif (39). Substrates that contain the LxxIxE motif bind to PP2A in the B56 hydrophobic pocket. The composition, phosphorylation, and charge of residues in the SLiM determines protein binding affinity for PP2A. Several viruses have evolved to target PP2A B56 through B56 substrate specificity for the LxxIxE motif. Hepatitis B virus, HIV-1, Ebola virus, and HTLV-1 hijack PP2A through the B56-binding LxxIxE motif to increase virus production. Previous studies have developed inhibitors that target the LxxIxE hydrophobic binding pocket, which interfered with Ebola virus production (40). Therefore, targeting HTLV-1 integrase-PP2A binding through the LxxIxE motif may reduce HTLV-1 replication or infectivity.

### 1.8 Integrase and PP2A B'56 $\gamma$ Subunit

HTLV-1 integrase binds to the host PP2A B'56 $\gamma$  subunit at the PP2AB' binding site (PP2AB'-BS) (34). The PP2AB'-BS is located in the flexible linker region between the CCD and CTD of the outer non-catalytic integrase subunits. One PP2A B'56 $\gamma$  co-factor protein binds to each outer non-catalytic subunit, which stabilizes each inner and outer subunit dimer. The outer non-catalytic CCD and CTD each bind to an end of the B'56 $\gamma$  protein concave structure. The integrase flexible linker region forms a U configuration with the conserved LxxIxE motif in the B'56 $\gamma$  binding pocket (Figure 3). The LxxIxE motif is essential for integrase-PP2A binding at the PP2AB'-BS. Previous studies have shown that the mutation of the integrase LQPIPE sequence to AQPAPA inhibits integrase-PP2A binding (34).

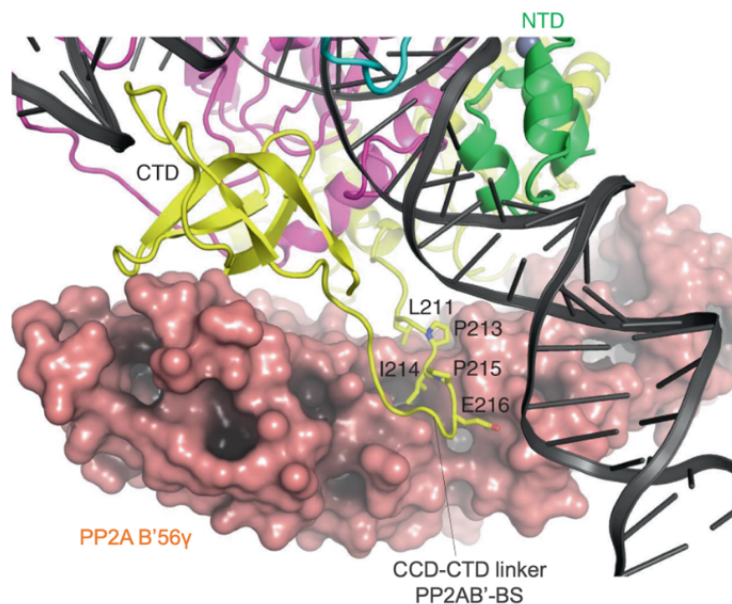


**Figure 3: Interaction between the integrase LxxIxE motif and the PP2A B'56 $\gamma$  subunit.**

The outer non-catalytic CTD and NTD are shown in yellow and green respectively. The highly conserved LxxIxE motif in the PP2AB'-BS is shown in the CCD-CTD flexible linker. The linker region forms a U-shaped conformation that facilitates binding with the concave host PP2A B'56 $\gamma$  subunit, shown in pink. The inner catalytic linker region shown in magenta extends across the PP2A surface. Viral DNA is shown in black. Figure is adapted from reference 34 (Bhatt *et al.*, 2022) (34).

Since mutations in the conserved LxxIxE motif are known to disrupt integrase-PP2A binding, the PP2AB'-BS is the focus of this study to explore novel non-catalytic integrase functions. L213A, I216A, and E218A mutations located in the CTD interfere with intasome assembly and B'56 $\gamma$  subunit binding; the D122N mutation within the CCD eliminates integrase activity, serving as a negative control (41). By introducing mutations in the highly conserved binding site, we establish stable virus producing cell lines and investigate the role of integrase-PP2A binding in viral particle production and viral infectivity. By inhibiting integrase-PP2A interaction, we characterize integrase's non-catalytic functions and explore the efficacy of therapeutic interventions that target this highly conserved binding site.

### **1.9 Hypothesis**

Based on this background, we hypothesize that the mutations (L213A, I216A, E218A) within the conserved LxxIxE motif of the PP2AB' binding site in viral integrase will affect the integration efficiency, infectivity, and viral production. Alanine substitutions at residues essential for integrase-PP2A binding will likely decrease infectivity compared to wildtype HTLV-1 virus.

## 2. MATERIALS AND METHODS

### 2.1 Mutant Virus and Cell Lines

Proviral, infectious molecular clones with wildtype (wt), L213A, I216A, E218A, and D122N integrase mutations were obtained from the Goedele Maertens Lab. Epithelial-like 293T cells and 729B human lymphoblastoid cells were purchased from the American Type Culture Collection.

L213A, I216A, E218A, D122N, and wt virus were used in this study. The plasmid DNA was transformed in *E. coli* to achieve more copies. Later, 729B cells were transfected with the respective plasmid, following puromycin selection, to obtain the transfected stable cells lines. Single cell cloning and ELISA were performed to measure viral p19 production in 729B-ACH cell clones. Clones producing high amounts of p19 were selected for further experiments. Moreover, 293T cells were infected with Derse's virus to characterize integration efficiency. The procedures are discussed in detail below.

### 2.2 Transforming *E. coli* with plasmid DNA

To transform *E. coli* and produce more copies of the wt, L213A, I216A, E218A, and D122N mutant virus, 30  $\mu$ L of *E. coli* and 1  $\mu$ L of plasmid DNA were combined in a 0.1 cm cuvette. The *E. coli* and plasmid DNA mixture were electroporated at 1.2 kV. After electroporation, 300  $\mu$ L of Super Optimal broth with Catabolite repression (S.O.C.) medium was added, and the mixture was shaken at 30°C for one hour for maximum transformation efficiency. The transformed *E. coli* cells were plated on 37 g/L Luria-Bertani (LB) agar plates with 100  $\mu$ g/mL ampicillin. Transformed single *E. coli* colonies were inoculated in sterile culture tubes containing 3 mL of autoclaved 25 g/L LB with 100  $\mu$ g/mL ampicillin.

### 2.3 Isolating plasmid DNA

A miniprep was performed to identify bacterial colonies that contain the transformed intact viral plasmid. The Invitrogen™ PureLink™ Quick Plasmid Miniprep Kit procedure and reagents were used for plasmid isolation. For each miniprep, 1 mL of the LB culture was centrifuged to harvest cells. Cell pellets were resuspended in 250  $\mu$ L of Resuspension Buffer, lysed in 250  $\mu$ L of Lysis Buffer, and precipitated in 350  $\mu$ L of Precipitation Buffer. After centrifugation, the supernatant was loaded onto a spin column and centrifuged to bind to the column. The column was washed with 700  $\mu$ L of Wash Buffer, and purified plasmid DNA was eluted in 50  $\mu$ L of warmed Tris EDTA (TE) buffer. After miniprep plasmid isolation, plasmid DNA concentration was measured using the BioTek Synergy HTX Multimode Reader. Purified plasmid samples with 6x New England BioLabs® loading dye were run on a 0.7% agarose gel in 1x Tris-acetate-EDTA (TAE) buffer. Plasmid samples were compared to the New England BioLabs® supercoiled DNA ladder to identify bacterial colonies that contained the intact 11 kb plasmid. Purified plasmids that contained the intact 11 kb plasmid were selected for midpreps (Figure 4).

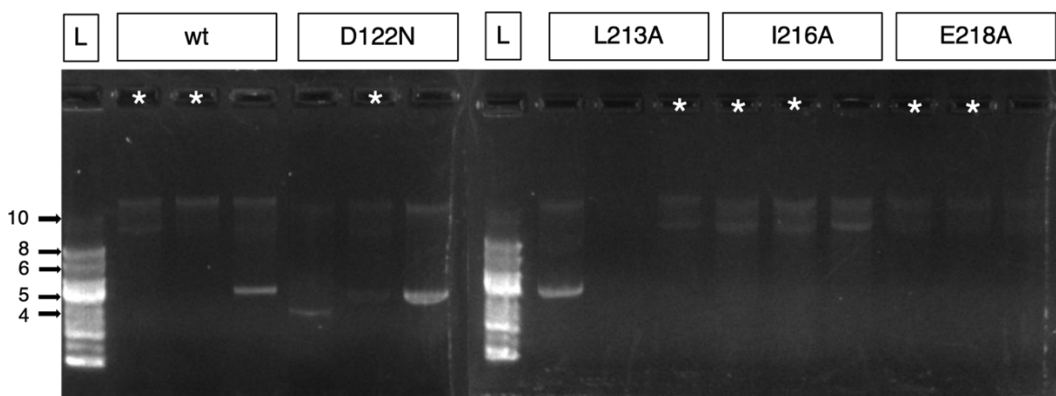


**Figure 4: Miniprep gel electrophoresis.**

Miniprep purified plasmids electrophoresed on a 0.7% agarose gel in 1x TAE buffer. Lane L contains supercoiled DNA ladder (New England BioLabs®). Wt, D122N, L213A, I216A, and E218A integrase mutants that contained the intact 11 kb viral genome are indicated with an asterisk.

After determining which bacterial cultures contained the full-length viral genome, overnight cultures with 400 mL 25 g/L LB, 1 mL of the miniprep culture, and 100 µg/mL ampicillin were prepared. The Invitrogen™ PureLink™ HiPure Plasmid Filter DNA Purification Kit procedure and reagents were used to isolate a greater quantity of plasmid DNA for cell transfections. For each midiprep, a PureLink™ HiPure Midi Column was prepared with 15 mL of EQ1 Equilibrium Buffer. Overnight cultures were centrifuged to harvest *E. coli* cells and cell pellets were resuspended in 10 mL of Resuspension Buffer (50 mM Tris-HCl, pH 8.0 and 10 mM EDTA) with RNase A (20 mg/mL). After adding 10 mL of Lysis Buffer (0.2 M NaOH and 1% SDS) and 10 mL of Precipitation Buffer (3.1 M Potassium acetate, pH 5.5), the mixture was transferred to a vertical column to clarify the lysate. The columns were washed with 20 mL of Wash Buffer (0.1 M Sodium acetate, pH 5.0 and 825 mM NaCl) and eluted in 5 mL of Elution Buffer (100 mM Tris-HCl, pH 8.5 and 1.25 M NaCl). To precipitate the purified DNA, 3.5 mL of isopropanol was added. The DNA and isopropanol were centrifuged at 15,000 RPM for 30 minutes at 4°C. Cell pellets were washed with 5 mL of 70% ethanol and centrifuged at 15,000 RPM for 10 minutes at 4°C. The remaining cell pellets were dried in a 55°C oven and resuspended in 500 µL TE Buffer (10 mM Tris-HCl, pH 8.0 and 0.1 mM EDTA). Gel electrophoresis was used to confirm purified plasmid size and DNA concentration was determined using the same procedure described for minipreps (Figure 5). Plasmid DNA was stored at -20°C for the duration of experiments.

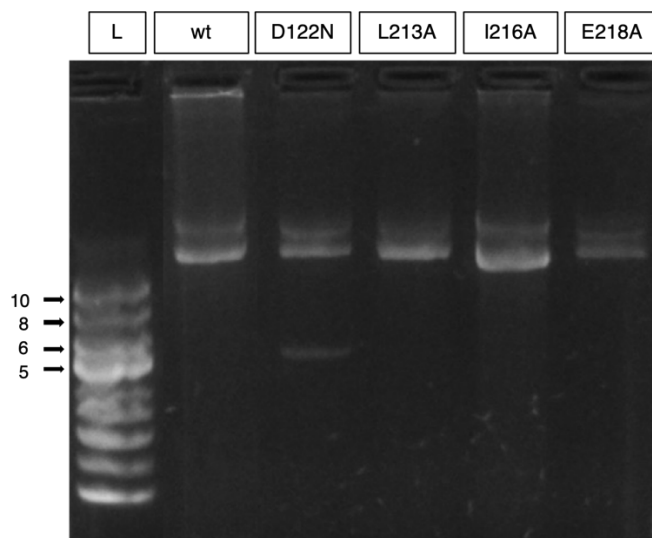


**Figure 5: Midiprep gel electrophoresis.**

Plasmids isolated in each midiprep were run on a 0.7% agarose gel in 1x TAE buffer. Lane L contains supercoiled DNA ladder (New England BioLabs®). The midiprep wt, D122N, L213A, I216A, and E218A samples contained the 11 kb plasmid.

## 2.4 Plasmid Linearization

To improve transfection efficiency, XmnI restriction digests were performed. Each digestion contained 10  $\mu$ g DNA, 10  $\mu$ L of New England BioLabs® 10x CutSmart® Buffer, 2  $\mu$ L of New England BioLabs® XmnI restriction enzyme, and deionized water for a 100  $\mu$ L total reaction volume. Digests were incubated for 2 hours at 37°C. Gel electrophoresis was used to confirm plasmid linearization using a New England BioLabs® 10kb DNA ladder as described above. Successful restriction digest products formed a 13kb band when electrophoresed. One successful gel of 10 $\mu$ g L213A restriction digests is shown in Figure 6. The linearized DNA was purified using the Zymo Research DNA Clean & Concentrator®-5 kit. To purify the DNA, a 5:1 ratio of DNA binding buffer:sample was added, and the mixture was centrifuged on a Zymo-Spin™ Column. The column was washed twice with 200  $\mu$ L of DNA Wash Buffer. Pure DNA was eluted in 15 $\mu$ L of 65°C elution buffer.

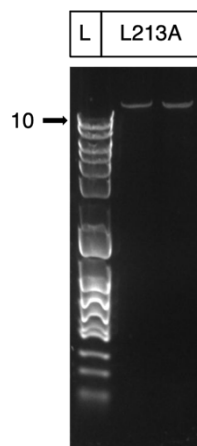


**Figure 6: XmnI plasmid linearization.**

L213A plasmids were digested with XmnI. The restriction digest products were visualized on a 0.7% agarose gel in 1x TAE buffer. Lane L contains 10kb DNA ladder (New England BioLabs®). Linearized plasmids formed a 13 kb band.

## 2.5 Transfecting 729B Cells

The Lonza Amaxa® Cell Line Nucleofector® Kit V was used to optimize transfections. For each transfection, 2 million 729B cells were resuspended in 82  $\mu$ L of Nucleofector Solution and 18  $\mu$ L of Supplement 1 with 2  $\mu$ g of plasmid DNA. The reaction mixture was transferred to a cuvette and secured in the Nucleofector™ II Transfection Device. The X-005 program was run on high expressivity mode. Immediately post nucleofection®, the contents of the cuvette were transferred to 5 mL pre-warmed RPMI media. After a 2-day recovery period, 12.5  $\mu$ g/mL blasticidin was added to the RPMI media. A kill curve was performed to determine the appropriate blasticidin concentration for antibiotic selection. Every 3 days, the media was replaced with fresh RPMI with 12.5  $\mu$ g/mL blasticidin to select for antibiotic resistant cells. Bulk transfected cells were progressively expanded.

## 2.6 p19 HTLV-1 ELISA assay

To determine which bulk cell lines were producing virus, p19 ELISA assays were performed using the ZeptoMetrix<sup>®</sup> HTLV p19 Antigen ELISA kit. The enzyme linked immunoassay detects HTLV-1 by reacting with p19, a major gag gene product. For each assay, a 96-well ELISA plate was coated with HTLV-1 patient serum diluted in 50mM sodium carbonate/bicarbonate buffer (pH 9.6) at a ratio of 1:250 and was incubated overnight at 4°C. To prepare the HTLV antigen standard, the 16 ng/mL antigen stock was serially diluted to 800 pg/mL, 400 pg/mL, 200 pg/mL, 100 pg/mL, 50 pg/mL, and 25 pg/mL in Assay Diluent. The supernatant (sup) from the cells in culture was diluted and lysed using 10x Lysis Buffer (1x PBS and 10% TX-100) for a final 1x concentration. The 96-well ELISA plate was washed four consecutive times with a 1x PBS, 0.1% Tween 20 Washing Buffer to remove the unbound patient serum. Either 200 µL of diluted standard or sample was added to each well and was incubated for 2 hours at 37°C, followed by a washing step as performed earlier. Later, 100 µL of 1:1000 biotin-p19 antibody diluted in 1% BSA dilution buffer was added to each well, and the plate was incubated for 1 hour at 37°C, followed by a washing step. After, 100 µL of 1:10,000 streptavidin-HRP was added per well. After a one-hour incubation period at 37°C, the plate was washed four times with Washing Buffer and 100 µL of Thermo Scientific<sup>™</sup> 1-Step<sup>™</sup> TMB ELISA Substrate Solution was added to each well. The ELISA plate was incubated at room temperature for approximately 20 minutes, until the standard dilutions were visibly blue after HRP catalyzed oxidation. After incubation, 100 µL of 4N sulfuric acid stop solution was added to each well. The ELISA plate was read using the BioTek Synergy HTX Multimode Reader at 450 nm.

## **2.7 Single Cell Cloning**

After determining which bulk 729B cell lines produced HTLV-1, serial dilutions were performed to obtain 729B-ACH single clones. Initial bulk cell concentrations were counted and 729B cells were serially diluted in RPMI media to plate one 96-well plate with 10 cells/well, one 96 well-plate with 1 cell/well and ten 96-well plates with 0.1 cell/well. Single cell clones were monitored for growth, indicated by a yellow RPMI media color change after media resources were metabolized. Color changes were observed between two and four weeks after single cell cloning. Cells from yellow wells on the 0.1 cell/well plates were expanded in 48-well plates.

## **2.8 Quantifying p19 Positive Single Clone Viral Particle Production**

After single cell cloning, several ZeptoMetrix® HTLV p19 Antigen ELISA assays were performed to identify virus producing clones as described above. Viral sup was collected from 1 million seeded cells after 48 hours in 1 mL RPMI. Positive clones were expanded and repeatedly tested to characterize p19 production. Three 729B-ACH clones were selected per mutant that showed high levels of p19 production. The three clones were maintained in culture for additional ELISA assays with 25 µg/mL phorbol 12-myristate 13-acetate (PMA) and 1 µM Ionomycin activation.

## **2.9 Infection assays**

Infection using the cell free virus: The recombinant HTLV-1-luc virus was produced by transfecting 293T cells with pHTLV-1-luc, pGag-pol and pVSVg plasmids. After 48 hours of infection, the cells were collected and luciferase activity was measured.

Infection by cocultivation: To assess infectivity, the 729B-ACH single cell clones were co-cultured with a Jurkat reporter cell line (JULR) expressing HTLV-1 LTR-luciferase. For each of the three selected 729B-ACH clones per integrase mutant,  $4 \times 10^6$  729B cells were co-cultured with  $1 \times 10^6$  JULR cells in 2 mL media for 48 hours. Later, 729B cells were separated from JULR by CD19 magnetic beads. Flow throw – CD19 negative cells (JULR) – were collected and cultured further. On day 7 and day 14,  $1 \times 10^6$  cells were collected for Digital Droplet PCR and  $1 \times 10^6$  cells were collected for Luc assay to measure the infectivity using the MGM Instruments Optocomp I Semi-Automatic Luminometer. Flow cytometry was performed to confirm CD19 negative JULR cells.

## **2.10 Confirming Integrase Mutation and Full-Length Viral Genome**

To confirm no significant deletions occurred thus far, DNA was isolated from 2 million 729B cells using the Qiagen DNeasy purification kit. Pelleted 729B cells were resuspended in 200  $\mu$ L of 1xPBS. After, 20  $\mu$ L of Proteinase K and 200  $\mu$ L of AL Lysis Buffer were added. Cells were incubated at 56°C for 10 minutes. After adding 200  $\mu$ L of 100% ethanol, the mixture was transferred onto a DNeasy mini spin column in a collection tube, centrifuged at 8000 rpm for 1 minute, and washed with 500  $\mu$ L of AW1 then AW2 buffer. DNA was eluted in 100  $\mu$ L EB buffer. The BioTek Synergy HTX Multimode Reader was used to determine DNA concentration.

For PCR to amplify the full-length viral genome, each reaction consisted of 10  $\mu$ L of 2xPCR Master Mix (150 mM Tris-HCl pH 8.5, 40 mM  $(\text{NH}_4)_2\text{SO}_4$ , 3 mM  $\text{MgCl}_2$ , 0.2% Tween 20, 4 mM dNTPs, 2 units/ $\mu$ L AS ONE Taq polymerase), 0.2  $\mu$ L of Tax 5' (50 $\mu$ M) primer, 0.2  $\mu$ L of LTR U3-R (50 $\mu$ M) primer, 5  $\mu$ L deionized  $\text{H}_2\text{O}$ , and 200-500  $\mu$ g isolated DNA. The PCR reaction amplified the viral genome between U5 of the 5' LTR and U3 of the 3' LTR (Figure 7).

To amplify the integrase gene to confirm the mutation, PCR reactions were prepared with 10  $\mu$ L of 2xPCR Master Mix, 0.2  $\mu$ L of ACH-4201F (50 $\mu$ M) primer, 0.2  $\mu$ L of ACH-5268R (50 $\mu$ M) primer, 5  $\mu$ L deionized H<sub>2</sub>O, and 5  $\mu$ L isolated DNA. PCR reactions were performed in the Bio-Rad T100 Thermal Cycler. Thermocycler conditions are listed in Table 1.

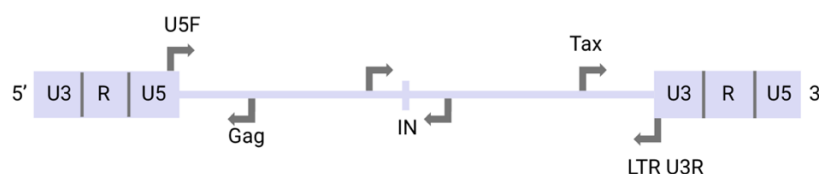


**Figure 7: Diagram of primers for HTLV PCR.**

The U5F and LTR U3R primers were used to amplify the full-length viral genome. The ACH-4201F and ACH-5268R internal primers were used to amplify the integrase gene (IN).

Thermocycler	Temperature ( $^{\circ}$ C)	Time
Initial Denaturation	95	30 sec
Denaturation	98	10 sec
Anneal	60	15 sec
Extension	68	10 min
Cycle Repeats – 35x		
Final Extension	68	10 min
Hold	12	$\infty$

**Table 1: Thermocycler conditions for PCR.**

Conditions were set on the Bio-Rad T100 Thermal Cycler to confirm the viral genome.

The amplified full length viral genome and integrase gene were electrophoresed on a 1% agarose gel in 1x TAE Buffer. The full-length viral genome was expected to form an approximately 8kb band when compared to a New England BioLabs<sup>®</sup> 10kb DNA ladder. The integrase gene was expected to form an approximately 1kb band and was compared to a 100 bp ladder.

The integrase gel DNA band was cut from the agarose gel and purified using the Zymoclean™ Gel DNA Recovery Kit for sequencing. Three volumes of Agarose Dissolving Buffer were added to each gel band. The gel and dissolving buffer were incubated at 56°C for 10 minutes and centrifuged for 30 seconds at maximum speed in a Zymo-Spin Column. Columns were washed with 200 µL of DNA Wash Buffer and DNA was eluted in 15 µL Tris-HCl (pH 7.5). Isolated integrase DNA was sequenced by Azenta Life Sciences to confirm L213A, I216A, E218A, and D122N integrase mutations.

## 2.11 Western Blot

Western blots were performed to determine p19, p24 and integrase in the cells and supernatant of the selected clones from wildtype and integrase mutants. These proteins from the cells were normalized with GAPDH. For the supernatant, p19 was determined using ELISA so as to normalize and load equal amounts of p19 in the gel.

For Western blots,  $5 \times 10^6$  cells were collected and lysed using RIPA lysis buffer containing 1x protease inhibitor and 1x benzonase. Cell lysates were then vortexed for 20 minutes and sonicated for 30 seconds on/30 seconds rest for 20 cycles. Sonicated samples were centrifuged at maximum speed for 10 minutes at 4°C. The supernatant for each sample was mixed with 6x loading buffer, boiled for 8 minutes and loaded on a separation and stacking gel with 1xSDS running buffer. Separation gels (10%) were prepared with H<sub>2</sub>O, 1.5 M Tris HCl (pH 8.8), 30% Acrylamide, 10% SDS, 10% APS, and Tetramethylethylenediamine (TEMED). After the separation gel polymerized, the stacking gel (4.5%) was prepared with H<sub>2</sub>O, 1 M Tris HCl (pH 6.8), 30% Acrylamide, 10% SDS, 10% APS, and TEMED.

Gels were run at 85V until the sample passed through the stacking gel. Samples were subsequently electrophoresed at 120V. After samples passed through the separation gel,

Immobilon®-P PVDF Transfer Membranes were activated in methanol and washed in 1xTransfer Buffer diluted from VWR® Life Science 10X Rapid Transfer Buffer. Gels were transferred onto activated transfer membranes using the Bio-Rad gel holder cassette and foam pads and were electrophoresed at 85V for 30 minutes at 4°C in 1x Transfer Buffer. Membranes were blocked for 1 hour at room temperature with blocking buffer containing 5% milk in Tris-Buffered Saline with 0.1% Tween 20 Detergent (TBST). Later the membrane was stained with 1:1000 primary antibody and washed three times with TBST over 25 minutes. Membranes were incubated with secondary antibody with a 1:10,000 dilution in TBST, followed by washes. Blots were then visualized using Biorad ECL substrate.

### 3. RESULTS

#### 3.1 Establishing stable 729B-ACH cell lines that produce infectious HTLV-1 virus

##### Examination of viral production by p19 ELISA

We established 729B-ACH single cell lines with mutations in the highly conserved LxxIxE integrase-PP2A binding site to determine if disrupting integrase-PP2A binding affects viral particle production. To test our hypothesis, we generated more than 226 single cell lines that had significant p19 protein production. Three clones for each wildtype or mutant virus with consistently high levels of p19 production were selected. Viral particle production for the three clones were repeatedly characterized using a p19 ELISA assay. Clones were activated with 25  $\mu\text{g/mL}$  phorbol myristate acetate (PMA) and 1  $\mu\text{M}$  ionomycin to stimulate p19 production. As shown in Figure 8, viral production tended to increase after activation, except for E218A mutants. E218A mutants had the lowest p19 production both with and without activation.

In the p19 ELISA assay, the wildtype clones produced between 1.53-2.55 ng/mL p19. The D122N p19 production ranged between 1.15-3.65 ng/mL. L213A produced between 0.74-3.175 ng/mL p19, and I216A produced between 2.99-4.56 ng/mL p19. E218A clones had the lowest p19 production levels, ranging between 0.33-1.54 ng/mL. After PMA and ionomycin activation, wildtype p19 production increased to 2.7-4.6 ng/mL. D122N viral particle production ranged between 3.1-9 ng/mL. L213A p19 production increased to 2.5-3.2 ng/mL, and I216A p19 production ranged between 5.2-6.6 ng/mL. E218A p19 production was consistently low at 0.2-0.4 ng/mL.

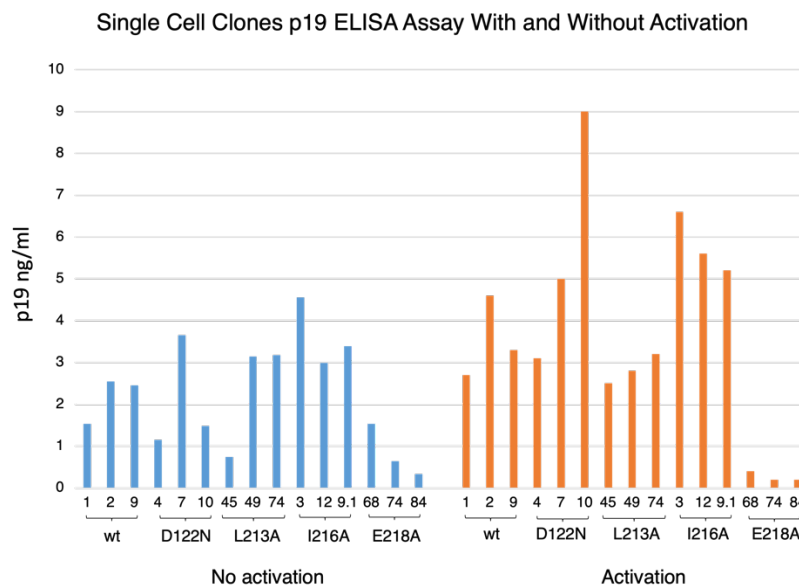


**Figure 8: Viral production from 729B-ACH single cell clones as measured by p19 ELISA with and without PMA and Ionomycin activation.**

One million stable 729B-ACH cells were cultured in 2mL RPMI medium for 48 hours and the supernatant was collected to quantify the viral production by p19 ELISA. Three established cell clones as indicated by clone numbers for each mutant or wildtype virus were tested with and without PMA and Ionomycin activation.

#### Infectivity assessment by cell-cell contact infection assay

To further test if the single cell clones produced infectious virus particles, 729B-ACH clones were co-cultured with Jurkat-luc (LTR-Luc) reporter cells. Viruses produced by 729B-ACH clones infect the reporter cells through cell-to-cell contact, and tax protein synthesized by newly infected virus drives luciferase production in reporter cells. According to Figure 9, other than E218A clones, all wt, D122N, L213A, and I216A clones generated substantial viral particles both with and without PMA and Ionomycin activation as judged by Tax driven luciferase activity in reporter cells, indicating that the viruses produced from the 729B-ACH clones are infectious and the cell lines can be used for future *in vitro* and *in vivo* studies.

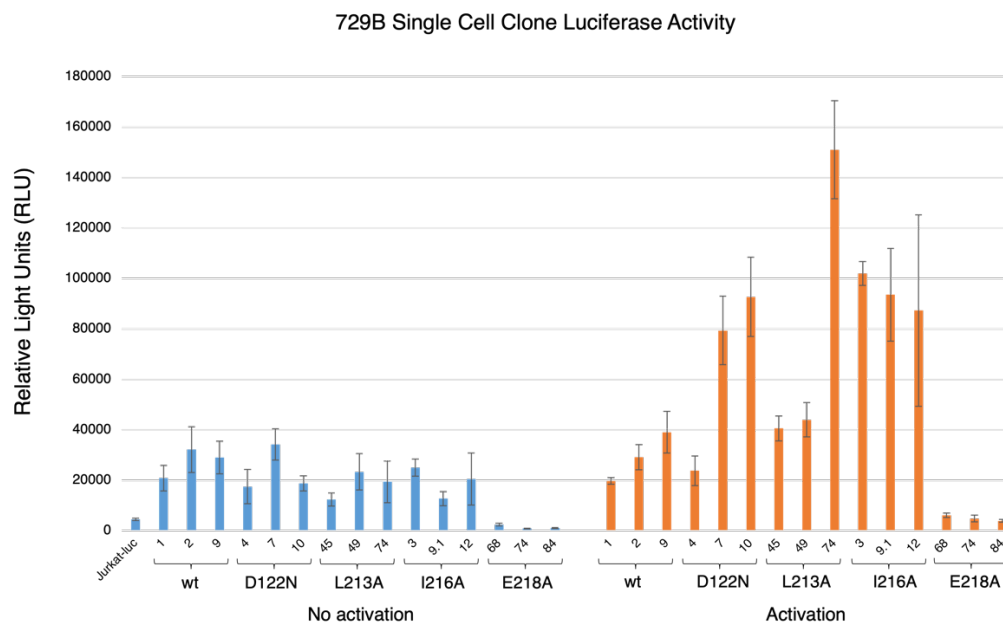


**Figure 9: The 729B-ACH cell clones produce infectious HTLV-1 virus.**

729B-ACH cells were co-cultured with Jurkat-luc reporter cells for 48 hours and the cells were collected, lysed and tested for luciferase activity presented as RLU. Three repeats were run for each cell clone. 729B-ACH clone luciferase activity errors bars represent  $\pm 1$  standard deviation.

### 3.2 The 729B-ACH cell clones carry the full length proviral genome and correct integrase gene sequence.

Since our goal was to investigate how LxxIxE binding site mutations affect virus production and infectivity, we confirmed that the 729B-ACH clones contained the intact proviral genome and correct integrase mutation (D122N, L213A, I216A, E218A). After characterizing the three 729B-ACH clones for each wildtype or integrase mutant, PCR was used to amplify the full-length viral genome from the 5' U5 to 3' U3. According to Figure 10, all clones formed the approximately 8 kb band, the full length of the viral genome which suggests there were no major insertions or deletions while cells were maintained in culture.

After confirming there were no major insertions or deletions in the proviral genome, the integrase gene of each 729B-ACH clone was amplified by PCR to confirm the specific mutation.

All clones formed the approximately 1 kb band, and DNA sequencing (Azenta Life Sciences) confirmed wildtype integrase and the L213A, I216A, E218A, and D122N integrase mutations. The gel visualizing the wt integrase PCR product was representative of all integrase gene visualizations and is included for reference in Figure 11. The confirmation of the full length proviral genome and integrase gene sequence supports that the clones are suitable candidates for future *in vitro* and *in vivo* experiments.

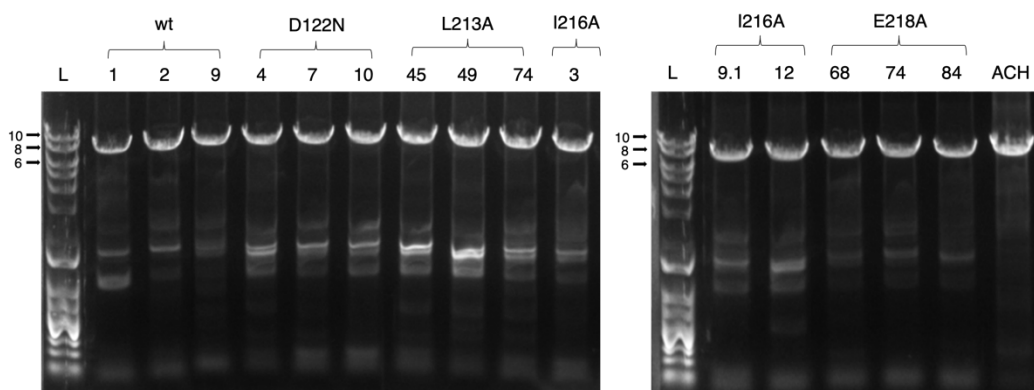


**Figure 10: PCR confirming full length proviral genome.**

Total DNA was isolated from each 729B-ACH cell clone and PCR was performed to amplify the full-length viral genome between the 5' LTR U5 and 3' LTR U3 as described in Methods. PCR products were electrophoresed on 1% agarose gel in 1x TAE Buffer. Lane L contains 10kb DNA ladder (New England BioLabs®). Control ACH plasmid is included in the final lane for comparison.

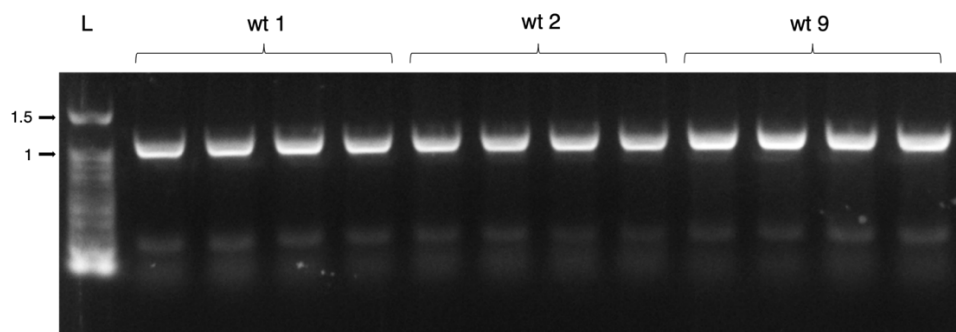


**Figure 11: PCR confirming integrase gene in 729B-ACH clones.**

Total DNA was isolated from each cell clone and PCR was performed to amplify the integrase gene. PCR products were electrophoresed on 1% agarose gel in 1x TAE Buffer. Bands formed at approximately 1kb and were excised from the gel, purified, and sequenced to confirm the correct integrase gene sequence. Lane L contains 100 base pair DNA ladder.

### 3.3 The mutations in the integrase LxxIxE motif inhibit HTLV-1 infection.

Since mutations in the conserved LxxIxE motif are known to disrupt integrase-PP2A binding, alanine substitutions at residues essential for integrase-PP2A binding (L213A, I216A, E218A) will likely affect the integration efficiency, infectivity, and viral production. To assess our hypotheses, 293T cells were infected with the recombinant HTLV-1-luc virus carrying the mutation and luciferase activity was then measured to evaluate the viral infectivity. As shown in Figure 12, all three mutations (L213A, I216A, E218A) significantly reduced the viral infectivity to the same level as the negative control D122N, the mutation abolishing the catalytic function of integrase.

A two-sample, two-tailed T-test was used to compare wildtype, L213A, I216A, and E218A luciferase activity with the D122N negative control to test for defects in integration. Wildtype clone luciferase activity was significantly different from the negative control ( $p=0.019$ ). L213A, I216A, and E218A mutant luciferase activity did not significantly differ from D122N activity ( $p=0.756$ ,  $p=0.319$ ,  $p=0.642$ ). Therefore, the L213A, I216A, and E218A integrase mutation likely caused a defect in integration, inhibiting viral infection.

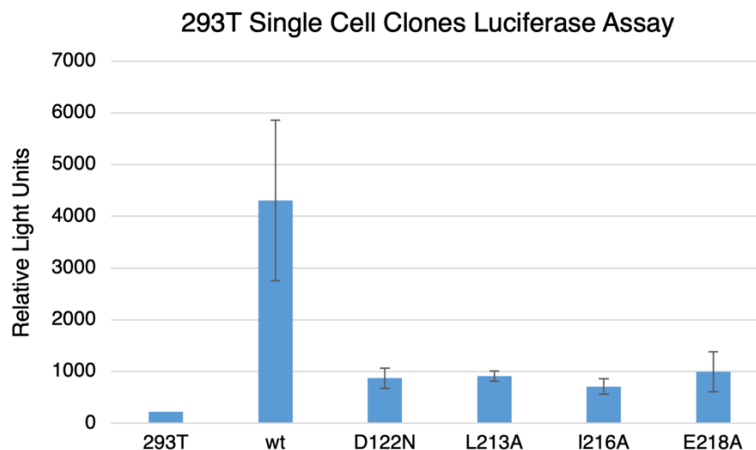


**Figure 12: The integrase mutations significantly reduce HTLV-1 infectivity.**

293T cells were infected with the same amount of various HTLV-1-luc viruses carrying the indicated integrase mutations for 48 hours. The cells were collected, and luciferase activity was measured, presented as RLU for viral infectivity. Three repeats were run for each viral infection. The 729B-ACH cell clones luciferase activity errors bars represent  $\pm 1$  standard deviation.

To confirm the above result further, we also performed an assay by co-culturing the 729B-ACH cell clones with Jurkat-luc reporter cells. As shown in Figure 13, the two mutant clones L213A #74 and I216A #9.1 significantly reduced the viral infectivity to the same level as the negative control D122N #10, which is consistent with the above result (Figure 12). Thus, the mutations cause a defect in viral integration and thereby inhibit HTLV-1 infection.

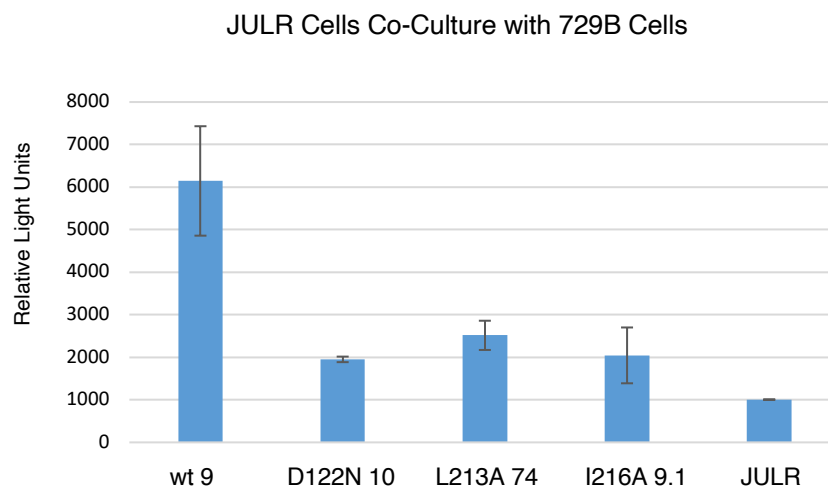
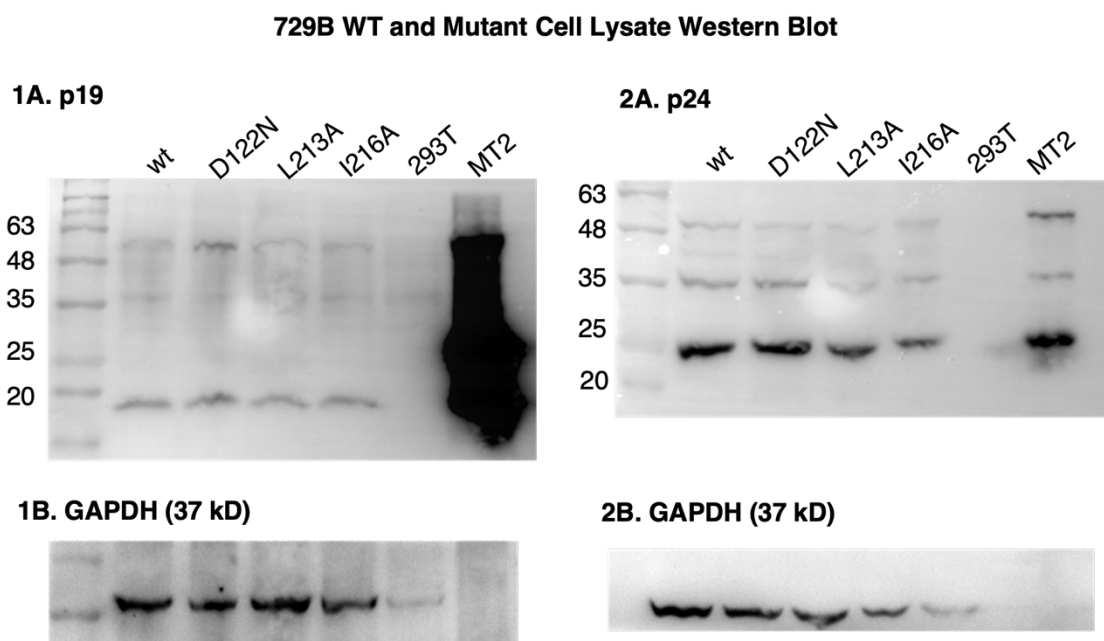


**Figure 13: The integrase mutations significantly reduce HTLV-1 infectivity in co-culture assay.** Jurkat-luc reporter cells were infected by coculturing with 729B-ACH cell clones (WT or mutants). After 48 hr of co-culture, Jurkat-luc cells were separated by removing 729B-ACH cells using CD19 beads. The isolated Jurkat-luc cells were cultured further for 7 days and the luciferase activity was measured and presented as RLU.

### 3.4 The integrase mutations of the provirus did not change the viral protein synthesis and packaging in 729B-ACH cell clones.

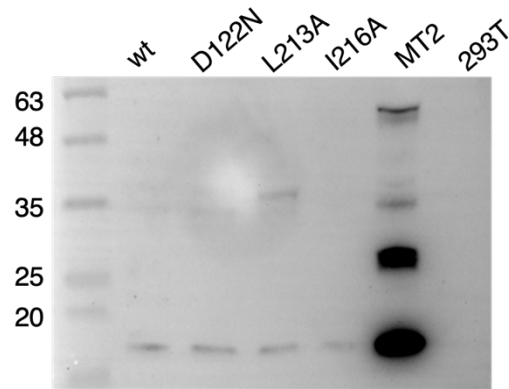
Since the LxxIxE binding motif facilitates integrase-PP2A binding, we investigated if binding site mutations affect viral protein synthesis and packaging in 729B-ACH clones. To visualize 729B-ACH clone protein synthesis and packaging, Western blots were performed on cell lysates and the viral particles produced from the cell clones. The MA (p19) and capsid (p24) viral protein concentrations in 729B-ACH D122N, L213A, and I216A cell lysates were compared to wildtype, 293T negative control, and MT2 positive control cell lines. The Western Blots were normalized with the GAPDH housekeeping gene. According to Figure 14, the 729B-ACH cell clones with integrase mutations did not show significantly different p19 or p24 synthesis from cells with wildtype virus. The MA (p19) in the mutant virus was also compared

with the wt virus. According to Figure 15, the 729B-ACH cell clones that contain the binding site mutation produced virus with a similar amount of MA (p19) as the wildtype virus. As shown in Figures 14 and 15, there were no substantial differences in viral protein production and packaging for 729B-ACH cells with and without LxxIxE motif mutations.



**Figure 14: Examination of the HTLV-1 proteins synthesized in 729B-ACH cell clones.**

Wildtype and mutant cells were collected and lysed for Western blots as described in Methods. Wildtype, D122N, L213A, I216A, 293T (negative control) and MT2 (positive control) cell lines were blotted to detect viral p19 (shown in 1A) and p24 protein (shown in 2A). GAPDH housekeeping protein (37 kD) was included as an internal control (shown in 1B and 2B).

**729B WT and Mutant Viral Supernatant p19 Western Blot**

**Figure 15: Examination of the MA (p19) in HTLV-1 viral particles produced from 729B-ACH cell clones.**

The medium was collected from the wildtype or mutant cell culture. The virus was concentrated and lysed for Western blots as described in Methods. Western Blot was performed to detect viral p19 in wt, D122N, L213A, I216A, MT2 (positive control), and 293T (negative control) cell supernatants.

## 4. DISCUSSION

In this study, we explore novel non-catalytic integrase functions to characterize the role of integrase-PP2A binding in HTLV-1 replication and infectivity. Previous studies have revealed that integrase binds to the PP2A B'56 $\gamma$  subunit via a highly conserved LxxIxE motif located in the CCD-CTD integrase linker region (34). Mutation of the L, I, and E residues has been shown to interfere with binding activity, and previous studies have found that integrase-PP2A binding is essential for intasome assembly and integration efficiency (34, 35). However, the consequences of abrogating binding for HTLV-1 replication and infectivity are not well understood.

The Goedele Maertens Lab's preliminary findings suggest that L213A, I216A, and E218A mutations cause defects in viral replication and infectivity compared to wildtype integrase virus. The Maertens group used green fluorescent protein to assess replication and infectivity for integrase mutants. In the current study, by using different assays our findings revealed similar replication and infectivity defects with the HTLV-1 mutants.

After transfecting 729B cells with mutant and wildtype virus, we successfully established more than 225 729B-ACH single cell lines that produced viral p19 protein. Several ELISA assays were performed to quantify p19 production and to identify cell lines that produced comparably high amounts of virus. Three 729B-ACH clones were selected for each mutant or wildtype virus and were repeatedly tested to monitor p19 production. When 729B-ACH clones were maintained for increased durations in culture, p19 production tended to decrease. The decrease in virus production over time may be due to the cytotoxicity of HTLV-1 or the selection of cells that have lower expression of viral products.

Both p19 ELISA assays and tax-driven luciferase assays provided evidence that wt, D122N, L213A, and I216A 729B-ACH single cell clones had significant virus production and

are reasonable candidates for future *in vitro* and *in vivo* studies. E218A clones had particularly low p19 production and tax-driven luciferase activity, suggesting that E218A clones are not suitable candidates for an *in vivo* study.

### Future Work

To expand on our findings, we will investigate if PP2A binding affects integration site specificity using next generation sequencing. Previous studies have investigated if CCCTC-binding factor (CTCF), a zinc finger protein that binds to HTLV-1 provirus, affects the selection of proviral integration sites (42). The study used next generation sequencing techniques to determine if CTCF binding affects integration preferences near active transcription start sites, CTCF sites, and CpG islands. The researchers found wildtype HTLV-1, HTLV-1 $\Delta$ CTCF, and a control HTLV-1 with a premature stop codon in the p12 protein did not have significantly different HTLV integration site specificity. We will utilize similar methodology to determine if PP2A binding affects integration site specificity.

We have begun to further explore integrase-PP2A binding through a CRISPR/Cas9 knockout (KO) of the PP2A B'56 $\gamma$  subunit that typically facilitates binding. We used recombinant HTLV-1-luc virus to infect 293T $\Delta$ PP2A or 293T $\Delta$ PP2A with PP2A re-expressed cell lines. Preliminary results suggest that PP2A B'56 $\gamma$  gene deletion by CRISPR/Cas9 in 293T cells resulted in inhibition of viral infection and re-expression of PP2A may rescue wildtype phenotype.

In future studies, we will infect humanized mice with our mutant and wildtype viral clones to monitor disease progression. We anticipate that humanized mice infected with L213A or I216A mutant virus will exhibit slower or even no disease progression compared to mice infected with wildtype virus. Based on our *in vitro* studies, the L213A and I216A mutations

caused defects in integration. Therefore, we hypothesize that the binding site mutant viruses will reduce pathogenesis. This study may provide supporting evidence for HTLV-1 interventions that target integrase-PP2A binding *in vivo*.

## References

1. Miura M, Naito T, Saito M. 2022. Current Perspectives in Human T-Cell Leukemia Virus Type 1 Infection and Its Associated Diseases. *Frontiers in Medicine* 9:1-10.
2. Hron T, Ellede D, Gifford RJ. 2019. Deltaretroviruses have circulated since at least the Paleogene and infected a broad range of mammalian species. *Retrovirology* 16.
3. Buehring GC, Shen HM, Jensen HM, Choi KY, Sun D, Nuovo G. 2014. Bovine Leukemia Virus DNA in Human Breast Tissue. *Emerging Infectious Diseases* 20:772-782.
4. Wolfe ND, Heneine W, Carr JK, Garcia AD, Shanmugam V, Tamoufe U, Torimiro JN, Prosser AT, LeBreton M, Mpoudi-Ngole E, McCutchan FE, Birx DL, Folks TM, Burke DS, Switzer WM. 2005. Emergence of unique primate T-lymphotropic viruses among central African bushmeat hunters. *PNAS* 102:7994-7999.
5. Bryan ES, Tadi P. 2023. Human T-Cell Lymphotropic Virus. StatPearls Publishing LLC, Treasure Island (FL).
6. Poiesz BJ, Ruscetti FW, Gazdar AF, Bunn PA, Minna JD, Gallo RC. 1980. Detection and isolation of type C retrovirus particles from fresh and cultured lymphocytes of a patient with cutaneous T-cell lymphoma. *PNAS* 77:7415-7419.
7. Paiva A, Casseb J. 2015. Origin and Prevalence of Human T-Lymphotropic Virus Type 1 (HTLV-1) and Type 2 (HTLV-2) Among Indigenous Populations in the Americas. *Revista do Instituto de Medicina Tropical de São Paulo* 57:1-13.
8. Burns DS, Lamb L. 2023. Chapter 3 - Specific Infectious Diseases. *In* Chambers J (ed), *Field Guide to Global Health & Disaster Medicine* doi:<https://doi.org/10.1016/B978-0-323-79412-1.00003-5>. Elsevier.
9. Mahieux R, Gessain A. 2009. The human HTLV-3 and HTLV-4 retroviruses: New members of the HTLV family. *Pathologie Biologie* 57:161-166.
10. Miura M, Naito T, Saito M. 2022. Current Perspectives in Human T-Cell Leukemia Virus Type 1 Infection and Its Associated Diseases. *Frontiers in Medicine* 9.
11. Durer C, Babiker HM. 2023. Adult T-Cell Leukemia. StatPearls Publishing, Treasure Island (FL).
12. Saito M. 2014. Neuroimmunological aspects of human T-cell leukemia virus type 1-associated myelopathy/tropical spastic paraparesis. *Journal of NeuroVirology* 20:164-174.
13. Yonekura K, Utsunomiya A, Seto M, Takatsuka Y, Takeuchi S, Tokunaga M, Kubota A, Takeda K, Kanzaki T. 2015. Human T-lymphotropic virus type I proviral loads in patients

- with adult T-cell leukemia–lymphoma: Comparison between cutaneous type and other subtypes. *The Journal of Dermatology* 42:1143-1148.
14. Olindo S, Cabre P, Lézin A, Merle H, Saint-Vil M, Signate A, Bonnan M, Chalon A, Magnani L, Cesaire R, Smadja D. 2006. Natural history of human T-lymphotropic virus 1-associated myelopathy: a 14-year follow-up study. *Arch Neurol* 63:1560-1566.
  15. Tanaka T, Sekioka T, Usui M, Imashuku S. 2015. Opportunistic Infections in Patients with HTLV-1 Infection. *Case Reports in Hematology* 2015:943867.
  16. Gessain A, Cassar O. 2012. Epidemiological Aspects and World Distribution of HTLV-1 Infection. *Frontiers in Microbiology* 3.
  17. Eusebio-Ponce E, Anguita E, Paulino-Ramirez R, Candel FJ. 2019. HTLV-1 infection: An emerging risk. Pathogenesis, epidemiology, diagnosis and associated diseases. *Rev Esp Quimioter* 32:485-496.
  18. Martel M, Gotuzzo E. 2022. HTLV-1 Is Also a Sexually Transmitted Infection. *Frontiers in Public Health* 10.
  19. Kaula DR, Davis JA, the AST Infectious Diseases Community of Practice. 2013. Human T Cell Lymphotropic Virus 1/2 in Solid Organ Transplantation. *American Journal of Transplantation* 13:355-360.
  20. Roc L, de Mendoza C, Fernández-Alonso M, Reina G, Soriano V. 2019. Rapid subacute myelopathy following kidney transplantation from HTLV-1 donors: role of immunosuppressors and failure of antiretrovirals. *Therapeutic Advances in Infectious Disease* 6:1-8.
  21. Pais-Correia A-M, Sachse M, Guadagnini S, Robbiati V, Lasserre R, Gessain A, Gout O, Alcover A, Thoulouze M-I. 2010. Biofilm-like extracellular viral assemblies mediate HTLV-1 cell-to-cell transmission at virological synapses. *Nature Medicine* 16:83-90.
  22. Sol-Foulon N, Sourisseau M, Porrot F, Thoulouze M-I, Trouillet Cl, Nobile C, Blanchet F, Bartolo Vd, Noraz N, Taylor N, Alcover A, Hivroz C, Schwartz O. 2007. ZAP-70 kinase regulates HIV cell-to-cell spread and virological synapse formation. *The Embo Journal* 26:516-526.
  23. Prooyen NV, Gold H, Andresen V, Schwartz O, Jones K, Ruscetti F, Lockett S, Gudla P, Venzon D, Franchini G. 2010. Human T-cell leukemia virus type 1 p8 protein increases cellular conduits and virus transmission. *PNAS* 107:20738–20743.
  24. Pique C, Jones KS. 2012. Pathways of cell–cell transmission of HTLV-1. *Frontiers in Microbiology* 3:1-14.
  25. Boxus M, Willems L. 2009. Mechanisms of HTLV-1 persistence and transformation. *British Journal of Cancer* 101:1497–1501.

26. Verdonck K, González E, Dooren SV, Vandamme A-M, Vanham G, Gotuzzo E. 2007. Human T-lymphotropic virus 1: recent knowledge about an ancient infection. *The Lancet Infectious Diseases* 7:266-281.
27. IARC Working Group on the Evaluation of Carcinogenic Risks to Humans. 2012. *Biological Agents: A review of human carcinogens, vol 100 B*. International Agency for Research on Cancer, Lyon, France.
28. Hare S, Maertens GN, Cherepanova P. 2012. 3'-Processing and strand transfer catalysed by retroviral integrase in crystallo. *The Embo Journal* 31:3020–3028.
29. Melamed A, Laydon DJ, Gillet NA, Tanaka Y, Taylor GP, Bangham CRM. 2013. Genome-wide Determinants of Proviral Targeting, Clonal Abundance and Expression in Natural HTLV-1 Infection. *PLOS Pathogens* 9:1-13.
30. Engelman A, Cherepanov P. 2008. The Lentiviral Integrase Binding Protein LEDGF/p75 and HIV-1 Replication. *PLOS Pathogens* 4:1-9.
31. Nombela I, Michiels M, Looveren DV, Marcelis L, Ashkar Se, Belle SV, Bruggemans A, Tousseyn T, Schwaller J, Christ F, Gijsbers R, Rijck JD, Debyser Z. 2022. BET-Independent Murine Leukemia Virus Integration Is Retargeted In Vivo and Selects Distinct Genomic Elements for Lymphomagenesis. *Microbiology Spectrum* 10.
32. Maertens GN, Engelman AN, Cherepanov P. 2022. Structure and function of retroviral integrase. *Nature Reviews Microbiology* 20:20-34.
33. Flint SJ, Enquist LW, Krug RM, Racaniello VR, Shalka AM. 1999. *Principles of Virology : Molecular Biology, Pathogenesis, and Control*, 0 ed. American Society Microbiology.
34. Bhatt V, Shi K, Salamango DJ, Moeller NH, Pandey KK, Bera S, Bohl HO, Kurniawan F, Orellana K, Zhang W, Grandgenett DP, Harris RS, Sundborger-Lunna AC, Aihara H. 2020. Structural basis of host protein hijacking in human T-cell leukemia virus integration. *Nature Communications* 11.
35. Maertens GN. 2016. B'-protein phosphatase 2A is a functional binding partner of delta-retroviral integrase. *Nucleic Acids Research* 44:364-376.
36. Janssens V, Goris J. 2001. Protein phosphatase 2A: a highly regulated family of serine/threonine phosphatases implicated in cell growth and signalling. *Biochem J* 353:417-439.
37. Eichhorn PJA, Creighton MP, Bernards R. 2009. Protein phosphatase 2A regulatory subunits and cancer. *Biochimica et Biophysica Acta* 1795:1-15.
38. Wong HT, Luperchio AM, Riley S, Salamango DJ. 2023. Inhibition of ATM-directed antiviral responses by HIV-1 Vif. *PLOS Pathogens* 19.

39. Zhang Y, Jiang H, Yin H, Zhao X, Zhang Y. 2024. Emerging Roles of B56 Phosphorylation and Binding Motif in PP2A-B56 Holoenzyme Biological Function. *International Journal of Molecular Sciences* 25:3185.
40. Kruse T, Biedenkopf N, Hertz E, Dietzel E, Stalman G, López-Méndez B, Davey N, Nilsson J, Becker S. 2018. The Ebola Virus Nucleoprotein Recruits the Host PP2A-B56 Phosphatase to Activate Transcriptional Support Activity of VP30. *Molecular Cell* 69:136-145.
41. Barski MS, Minnell JJ, Hodakova Z, Pye VE, Nans A, Cherepanov P, Maertens GN. 2020. Cryo-EM structure of the deltaretroviral intasome in complex with the PP2A regulatory subunit B56 $\gamma$ . *Nature Communications* 11.
42. Cheng X, Joseph A, Castro V, Chen-Liaw A, Skidmore Z, Ueno T, Fujisawa J-i, Rauch DA, Challen GA, Martinez MP, Green P, Griffith M, Payton JE, Edwards JR, Ratner L. 2021. Epigenomic regulation of human T-cell leukemia virus by chromatin-insulator CTCF. *PLOS Pathogens* 17.